### Fjóla Jónsdóttir

Department of Mechanical and Industrial Engineering, University of Iceland, Reykjavik, Iceland e-mail: fj@hi.is

#### Glenn E. Beltz

e-mail: beltz@engineering.ucsb.edu

## Robert M. McMeeking

e-mail: mcm@engineering.usb.edu

Department of Mechanical and Environmental Engineering, University of California, Santa Barbara, CA 93106-5070

# Modeling of Threshold Strength in Cylindrical Ceramic Structures

Recently, three-dimensional structured ceramic composites with large threshold strengths (i.e., stress below which there is zero probability of failure) have been fabricated utilizing an architecture consisting of relatively stress-free, elongated prismatic domains, separated by thin compressive walls. We build upon prior work on laminate architectures, with the common feature that these structures are all susceptible to fracture. Typically, these three-dimensional structures consist of thin shells of mullite that surround alumina. Cracks, originating from large flaws within the ceramic body, are arrested by the surrounding compressive layers until a specific stress level is attained (i.e., the threshold strength), resulting in a truncation of the strength distribution in the flaw region. A preliminary stress intensity solution has shown that this arrest is caused by a reduction of the crack driving force by the residual compression in the compressive walls. This solution also predicts that the threshold strength is dependent not only on the magnitude of the residual compression in the walls but also on the dimensions of both phases. A finite element model is presented that utilizes a penny-shaped crack in the interior of such a structure or half-penny-shaped crack emanating from the edge of such a structure. Ongoing analytical and experimental work that is needed to more fully understand this arrest phenomenon and its application towards the development of reliable, damage-tolerant ceramic components are discussed. [DOI: 10.1115/1.1831296]

#### 1 Introduction

The major drawback of ceramics as structural materials is their brittleness. Brittle materials contain an unknown variety of cracks and flaws that are inadvertently introduced during processing and surface machining [1,2]. The high brittleness makes ceramic parts extremely prone to impact damage, often resulting in catastrophic failure. A concept which plays a central role in the study of crack arrest in brittle materials is the threshold strength—that is, a stress below which the probability of failure vanishes. This phenomenon increases the damage tolerance of ceramics and will allow engineers to design reliable ceramic components for structural applications. It has been shown by Rao et al. [3] and Hbaieb and Mc-Meeking [4,5], that thin compressive layers, within a laminar ceramic, arrest large cracks, and produce a threshold strength. These laminates have been shown to exhibit threshold strengths in accordance with finite element modeling of the crack propagation process. Typically, the laminar plates are composed of alternating layers of Al<sub>2</sub>O<sub>3</sub> and a mullite/Al<sub>2</sub>O<sub>3</sub> mixture. Residual compressive stresses in the layers can arise due to differential strain between the layers caused by one or more of the following: differential thermal contraction (or expansion) during cooling (or heating), a change in volume due to a crystallographic phase transformation, or molar volume change associated with the formation of a reaction product.

Since laminates are simply two-dimensional structures, they are only effective at arresting a crack in *one* direction. Three-dimensional structured ceramic composites have been fabricated that yield a threshold strength in other dimensions. This is being accomplished by assembling fibers and spheres using colloidal processing techniques and coating these geometries with another material. The coated fibers and spheres are then consolidated to produce a material with a periodic structure that includes layers in compression that can arrest cracks propagating in all three dimensions [6]. One type of three-dimensional structure consists of relatively stress-free, elongated prismatic domains, separated by thin compressive walls (see Fig. 1). This is the central idea underlying

Contributed by the Applied Mechanics Division of THE AMERICAN SOCIETY OF MECHANICAL ENGINEERS for publication in the ASME JOURNAL OF APPLIED MECHANICS. Manuscript received by the Applied Mechanics Division, June 30, 2003; final revision, July 9, 2004. Associate Editor: K. M. Liechti.

the present study. To understand the mechanics of fracture in this architecture, a simple analytic model and several finite element analyses are carried out to study the threshold strengths for different configurations.

Our analysis proceeds in the following way. First, the three-dimensional ceramic structure is simplified as an infinitely long cylindrical structure and a crack is modeled as a penny-shaped crack in the interior. The longitudinal axis of the cylinder is perpendicular to the plane of the crack and is assumed to nominally be in tension. The problem is then extended to a semi-infinite structure with a half-penny-shaped crack emanating from the edge of such a structure. Stress intensity factors are calculated for these two configurations as a crack grows from the tensile section into the compressive section. The stress intensity factors are used to determine the threshold stress, that is, the level needed to extend the crack through the compressive layers to produce catastrophic failure.

#### 2 Problem Formulation

The physical system that provides the basis for the following discussion is a three-dimensional architecture consisting of elongated prismatic domains, separated by thin compressive walls, as shown schematically in Fig. 1.

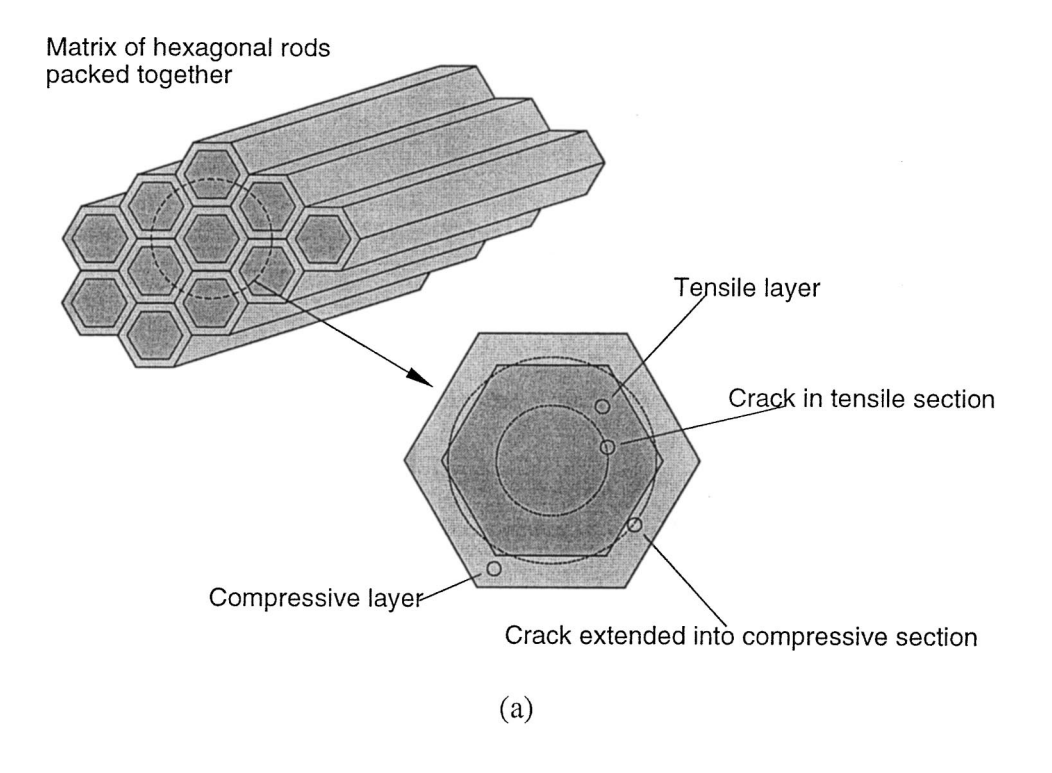
**2.1** Analytic Model for an Idealized Cylindrical Structure. As an approximation, we assume the three-dimensional architecture to be an infinitely long cylindrical structure. The structure consists of concentric cylinders, alternating between tensile and compressive zones, the innermost being a tensile zone. As a representative model, Fig. 2 shows three concentric cylinders with radii  $r_a$ ,  $r_b$ , and  $r_c$ , respectively. The thickness of the compressive layer is given by  $t=r_b-r_a$ . Assume a preexisting penny-shaped crack of diameter Fig. 2(a) spans the diameter of the tensile layer. In the following analyses, we determine the stress intensity factors for a crack when it extends into the compressive zone, that is, for  $r_a < a < r_b$ . The stress intensity factors are used to determine the applied threshold stress,  $\sigma_{thr}$ , needed to extend the crack through the compressive layers to produce catastrophic failure.

A stress intensity factor K can be determined by superimposing the two stress fields: the applied stress field and the residual stress

Journal of Applied Mechanics

Copyright © 2005 by ASME

MAY 2005, Vol. 72 / 381



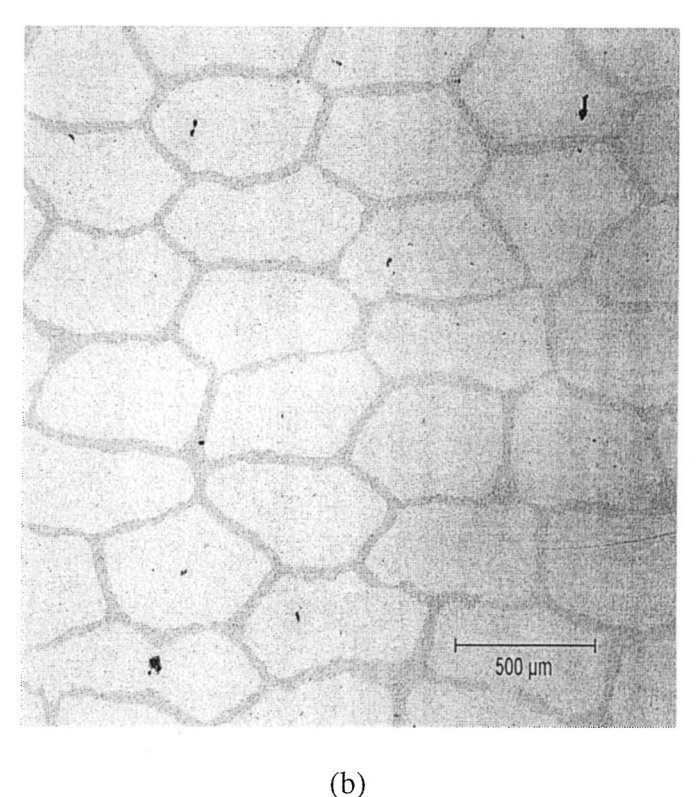


Fig. 1 (a) Schematic and (b) micrograph of a three-dimensional ceramic architecture. As a material example, the solid core consists of alumina  $(Al_2O_3)$ , while the thinner, compressive coating-like phase consists of a mixture of mullite and  $Al_2O_3$  (micrograph courtesy of M. Snyder).

field, as depicted in Fig. 3. Each stress field is applied to the same penny-shaped crack of diameter 2a and each has its own known stress intensity factor.

Before we carry out the superposition, let us assume that the cylindrical structure is infinitely long and subject only to uniform

tension,  $\sigma_a$ , at the remote boundary. The stress intensity factor for this case is readily available and given by Tada [7] as:

$$K_{\text{applied}} = 2 \sigma_a \sqrt{\frac{a}{\pi}} F(a/r_c),$$
 (1)

382 / Vol. 72, MAY 2005

Transactions of the ASME

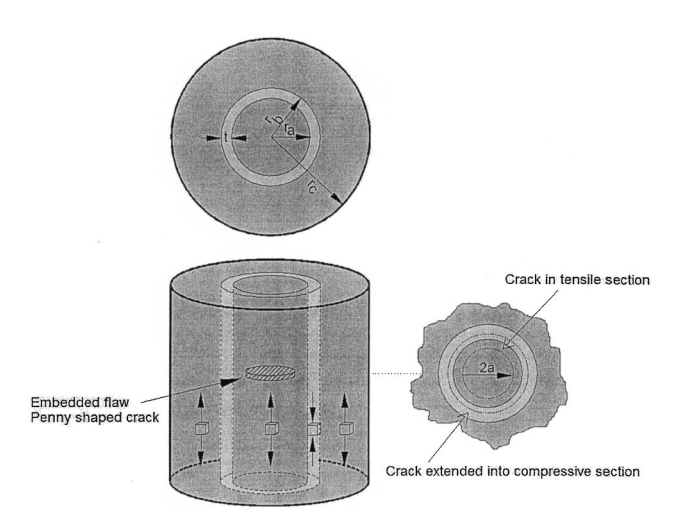


Fig. 2 Schematic of an infinite cylindrical structure containing a penny-shaped crack in its interior (tensile) phase

where  $F(a/r_c)$  is a dimensionless correction function given by:

$$F(a/r_c) \approx \frac{1 - 0.5 \frac{a}{r_c} + 0.148 \left(\frac{a}{r_c}\right)^3}{\sqrt{1 - \frac{a}{r_c}}}.$$
 (2)

The correction function depends on geometry of the structure and, as Eq. (2) shows, as radial dimension of the cylinder approaches infinity  $(r_c \rightarrow \infty)$ , the correction function approaches unity, that is  $F(a/r_c) \rightarrow 1$ . For purposes of this study, it is not feasible to use an infinite value for  $r_c$  and we must accept a finite value, which is reflective of the real three-dimensional structure. For our geometries, the magnitude of  $F(a/r_c)$  ranges from about 1.01 to about 1.375. The arbitrariness in the choice of  $r_c$ , which sets the background stress, is one disadvantage of the using cylindrical model to represent the stresses in what really is a periodic structure.

We now return our attention to the superposition scheme outline in Fig. 3. The applied stress is  $\sigma_a$ , the magnitude of the residual compression is  $\sigma_c$  (defined to be a positive number) and the residual tension is denoted as  $\sigma_t$ . The first stress field on the right-

hand side of the "equality" is a tensile stress of magnitude ( $\sigma_a - \sigma_c$ ), applied at the remote boundary, to a cracked specimen that does *not* contain residual stresses (with  $F \approx 1$ ). The stress intensity factor for this stress is given by the first term on the right side of Eq. (3). The second stress field is a tensile stress of magnitude ( $\sigma_c + \sigma_t$ ), applied only to the crack within the tensile region. Its stress intensity factor is given by the second term on the right side of Eq. (3). The two superimposed stress fields sum to that shown on the left-hand side of Fig. 3. The stress intensity factor for the two superimposed stress fields is thus given by:

$$K = (\sigma_a - \sigma_c) \frac{2}{\pi} \sqrt{\pi a} + \frac{2}{\sqrt{\pi a}} (\sigma_c + \sigma_t) \int_0^{r_a} \frac{\xi}{\sqrt{a^2 - \xi^2}} d\xi. \quad (3)$$

The integrand in Eq. (3) is due to a ring load of radius  $\xi$  which is integrated with intensity  $\sigma_t + \sigma_c$  up to a radius  $r_a$ . Evaluating the integral and simplifying gives:

$$K = 2\sigma_a \sqrt{\frac{a}{\pi}} + 2\sigma_t \sqrt{\frac{a}{\pi}} - 2(\sigma_c + \sigma_t) \sqrt{\frac{a}{\pi}} \sqrt{1 - \left(\frac{r_a}{a}\right)^2}. \quad (4)$$

The first term in Eq. (4) is recognized as the stress intensity factor for a penny-shaped crack in an applied tensile field, while the remainder of the expression is negative. Thus, the stress intensity factor initially decreases when the crack extends into the compressive shell of the material, and fracture resistance correspondingly increases. The analytical result in Eq. (4), for the stress intensity factor, is compared with calculated stress intensity factor, in Section 3.

Using elasticity theory, it can be shown that the magnitude of the axial tensile stress  $(0 < r < r_a \text{ and } r_b < r < r_c)$  is given by:

$$\sigma_t = \frac{E' \Delta \alpha \Delta T t (t + 2r_a)}{r_c^2},$$
 (5)

and, similarly, the magnitude of the axial compressive stress ( $r_a$  <r< $r_b$ ) is given by:

$$\sigma_c = \frac{E' \Delta \alpha \Delta T (r_c^2 - t^2 - 2tr_a)}{r_c^2},\tag{6}$$

where  $E' = E/(1 - \nu)$ , E is Young's modulus,  $\nu$  is Poisson's ratio,  $\Delta \alpha$  is the difference in thermal expansion between the two materials, and  $\Delta T$  is the temperature relative to a datum at which the

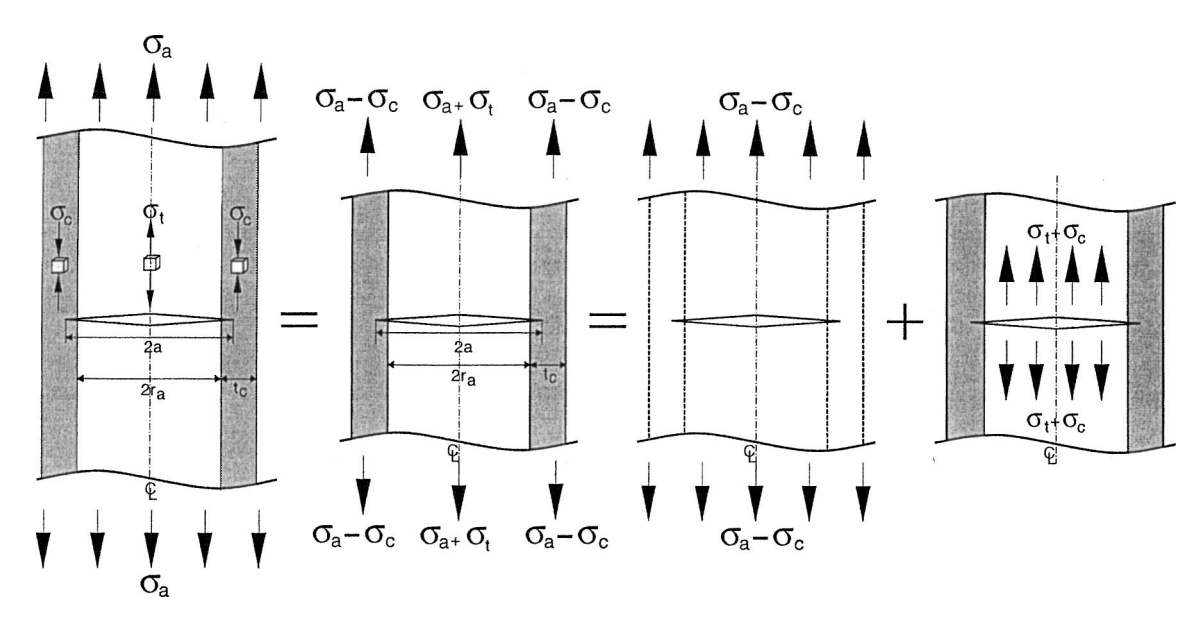


Fig. 3 Stresses in a loaded cylindrical ceramic architecture can be obtained via superposition

**Journal of Applied Mechanics** 

MAY 2005, Vol. 72 / 383

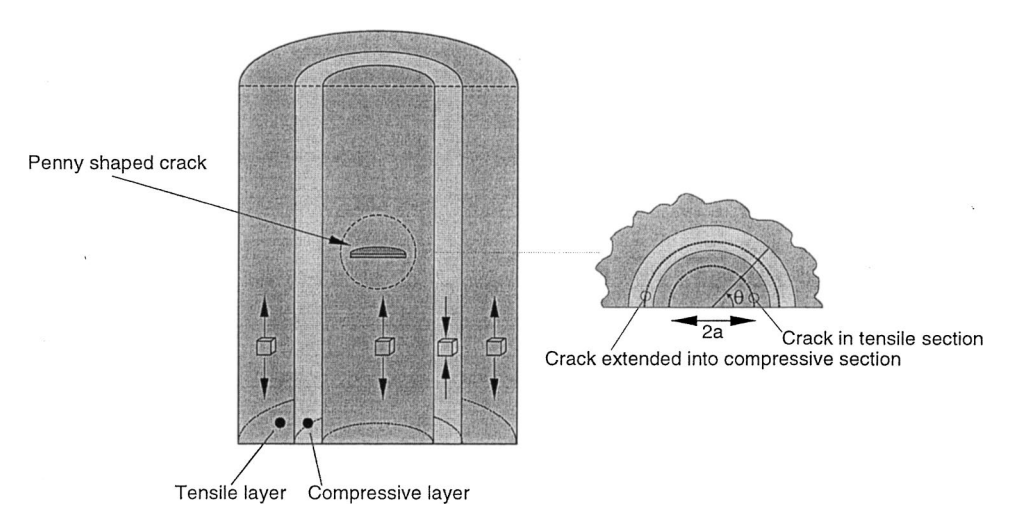


Fig. 4 Schematic of the semi-infinite cylindrical structure with a half-penny shaped crack emanating from the free surface

thermal residual stresses are zero. In Eqs. (5) and (6),  $\Delta \alpha \Delta T$  is taken to be a positive number. The derivation of Eqs. (5) and (6) is given in Appendix A.

In general, the stress intensity factor in Eq. (4) decreases monotonically as the crack grows through the compressive layer and, hence, the crack grows stably until it reaches the interface with the next tensile zone as the applied stress is increased. However, it can be shown that above a critical value of applied stress, the function K(a) reaches a local minimum in the compressive zone. If the crack were to reach this location, it would continue to grow unstably until reaching the interface with the tensile layer. Further discussion of this critical applied stress is given in Appendix B. In this paper, we avoid parameter regimes that lead to a minimum in K(a) prior to the crack reaching the tensile zone.

Assuming the threshold stress occurs when the crack has reached the interface with the tensile zone, one can identify K with  $K_c$  and a with  $r_a+t$  and solve for  $\sigma_a$  to arrive at:

$$\sigma_{thr} = \frac{K_c}{2} \sqrt{\frac{\pi}{r_a + t}} + \frac{\sigma_c t(t + 2r_a)}{t(t + 2r_a) - r_c^2} + \sigma_c \left(\frac{r_c^2}{r_c^2 - t(t + 2r_a)}\right) \sqrt{1 - \left(\frac{1}{1 + t/r_a}\right)^2}.$$
 (7)

By substituting Eq. (6) into (7) we can write the normalized threshold stress as:

$$\frac{\sigma_{thr}}{E'\Delta\alpha\Delta T} = \frac{K_c}{2E'\Delta\alpha\Delta T\sqrt{r_a}}\sqrt{\frac{\pi}{1+t/r_a}} - \left(\frac{r_a}{r_c}\right)^2 \left(\frac{t}{r_a}\right) \left(\frac{t}{r_a} + 2\right) + \sqrt{1 - \left(\frac{1}{1+t/r_a}\right)^2}.$$
 (8)

Equations (7) and (8) show that the threshold strength for a cylindrical composite increases with the fracture toughness of the thinlayer material, the magnitude of the compressive stress and the thicknesses of the various layers. These expressions are analogous to those worked out for laminate architectures in earlier work [3–5], in that they give very similar trends with regard to the variation of  $\sigma_{thr}$  with crack geometry. Most importantly, they allow one to design cylindrical ceramic architectures with the knowledge that failure will not occur below this value of stress.

This theoretical model ceases to apply when a variety of realistic effects prevail. For example, elastic mismatch is not accounted for; that is, we assume the effective Young's modulus E' is identical in both phases. In addition, we assume the crack

propagates radially on its original plane through the various phases. While this straight crack propagation has been observed to occur in many experiments, a phenomenon known as bifurcation can alternatively occur, where the crack may branch from its original plane after penetrating into the compressive layer [3]. This effect has been shown to increase the threshold strength beyond what is calculated here, but does imply that the physical mechanisms considered in this section are not universally applicable. While the finite element method discussed in the next section can be extended to consider cases that involve elastic modulus mismatch and bifurcation, we submit that the results presented in this work still provide invaluable guidance on the design of three-dimensional architectures that are fracture resistant. In addition, the current work provides a level of confidence before extending the FEM model to more complex geometries.

**2.2 Cracks Emanating From a Surface.** The second case we consider is a half of a concentric cylindrical structure with a half-penny-shaped crack emanating from the edge, as shown schematically in Fig. 4. The motivation for this geometry is that ceramic composites of this type are typically tested in bending, with surface cracks initiating from the surface in maximum tension.

For a half-space with a half-penny-shaped crack emanating from the edge and subject to tensile loading at the remote boundary, the stress intensity factor is well known and is given by Tada [7] as:

$$K = \frac{2}{\pi} \sigma_a \sqrt{\pi a} F(\theta), \tag{9}$$

where  $F(\theta)$  is given by:

$$F(\theta) \approx 1.211 - 0.186\sqrt{\sin \theta} \quad (10^{\circ} < \theta < 170^{\circ}).$$
 (10)

Given that we are using a finite value for the cylindrical diameter, the result by Tada can only be used as an approximation to our results.

Equations (9) and (10) show the stress intensity factor is dependent on the angle  $\theta$ , measured from the edge of the structure. However, this dependence is relatively weak. For a crack emanating from a free surface, the state of stress varies from plane strain in the interior of the plate to plane stress at the surface. Hence, using a crack-opening displacement method to calculate the stress intensity factors can give erroneous results so Eq. (10) is limited to internal angles. Raju and Newman [8] use a nodal-force method, which requires no prior assumption of either plane stress or plane strain, to obtain the stress intensity factors of semielliptical surface cracks. Their results seem to suggest that the stress

384 / Vol. 72, MAY 2005

Transactions of the ASME

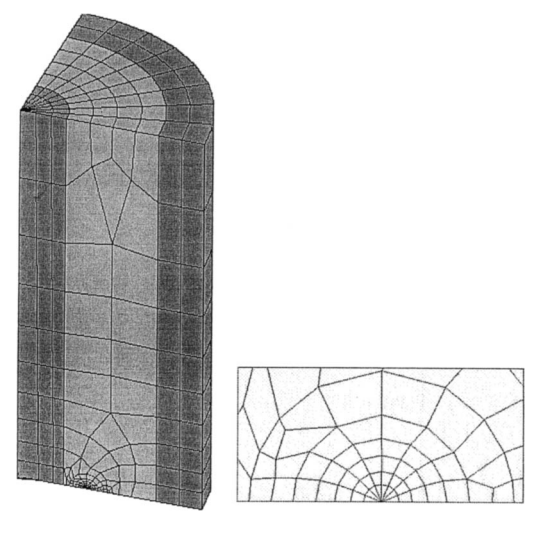


Fig. 5 Typical finite element model with singular elements around the crack tip

intensity factor varies strongly near the surface, indicating the need for substantial mesh refinement in this regime. Because of this complication we defer consideration of cracks at the point where they intersect the surface to future work.

For the case of residual stresses in a semi-infinite cylindrical structure there is no analytical solution available for stress intensity factors and we must rely solely on finite element analysis.

#### 3 FEM Models for Stress Intensity Factors

Stress intensity factors are calculated using the commercial finite element code ANSYS [9]. Recall the two cases considered; that is, an infinitely long cylindrical structure with a penny-shaped crack in the interior and a semi-infinite structure with a halfpenny-shaped crack emanating from the edge.

**3.1 Full Penny-Shaped Crack.** We first consider the structure of concentric cylinders with an embedded penny-shaped crack, as shown in Fig. 2. Figure 5 shows a typical finite element model with eight wedges. Given the symmetry of the problem, only one-eighth of the body is modeled. The 20-node brick elements are used in the analysis. The first row of elements around the crack tip is modeled with singular elements, with the midside nodes placed at the quarter points, to account for the  $r^{-1/2}$  singularity in stresses and strains at the crack tip. The stress intensity factors are calculated with a displacement extrapolation method as outlined in the ANSYS theory manual [9].

A typical dimension for the  $Al_2O_3$  tensile cells in the three-dimensional architecture is  $2r_a = 450 \, \mu \text{m}$ . For the compressive layers, a mixture of mullite and  $Al_2O_3$ , typical dimensions range from 23 to 90  $\, \mu \text{m}$  [10]. Two configurations are considered here: one in which the thickness of the compressive layer is equal to the diameter of the tensile cell, that is,  $t = 2r_a$ , and with  $2r_a = 200 \, \mu \text{m}$ ; one in which the compressive layer is one tenth the diameter of the tensile cell, that is,  $t = 2r_a/10$ , for a thickness of tensile layer  $2r_a = 450 \, \mu \text{m}$ . In the former,  $t/2r_a = 1$ , and in the latter,  $t/2r_a = 1/10$ . In both configurations, the elastic constants of the tensile and compressive zones are considered to be identical. The reason we choose two different thickness ratios is that the smaller one is comparable to the experimental dimensions used by Lange et al. [6,10] and the larger one is comparable to ratios used in finite element studies on laminates [4].

Figure 6 shows the calculated stress intensity factors for a thickness ratio of  $t/2r_a = 1$ . The results are plotted versus normalized crack length, as the crack extends from the tensile layer through the compressive layer. The results are shown separately for the stress intensity factor  $K_{\rm applied}$  due to the externally applied

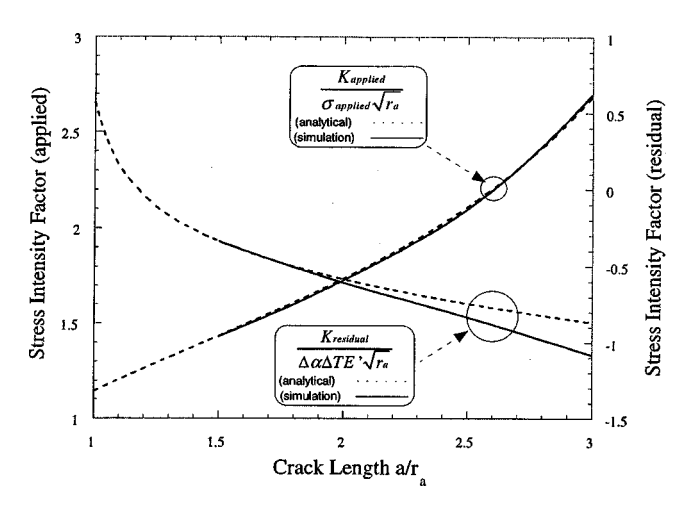


Fig. 6 Comparison of calculated and theoretical stress intensity factors. Tensile and compressive layers have equal thicknesses. Thickness of tensile layer is  $2r_a$ =200  $\mu$ m.

load, and for the stress intensity factor  $K_{\rm residual}$  due to the residual stress caused by thermal mismatch. The theoretical results for  $K_{\rm applied}$  and  $K_{\rm residual}$ , given by Eq. (4), are plotted on the same graph for comparison. As the figure shows, there is good agreement between the theoretical and computed results.

In Fig. 7, we show the calculated stress intensity factors for a thickness ratio of  $t/2r_a = 1/10$ . Again, the results are shown separately for  $K_{\rm applied}$  due to the externally applied load, and  $K_{\rm residual}$  due to the material mismatch. The theoretical results for  $K_{\rm applied}$  and  $K_{\rm residual}$  are plotted on the same graph for comparison. As in the previous case, there is good agreement between the theoretical and calculated results.

3.2 Half-Penny-Shaped Crack Emanating From the Surface. We next consider the second geometry—half of a cylindrical structure with a half-penny-shaped crack emanating from the edge, as shown in Fig. 4. The same two configurations are considered as for the full-penny-shaped crack, that is, a configuration where the thickness of the compressive layer is equal to the diameter of the tensile cell, and a configuration where the compressive layer is one tenth the diameter of the tensile cell. The finite element calculations are carried out in a similar fashion as in the previous section. Only one-fourth of the body is modeled, given the symmetry of the problem.

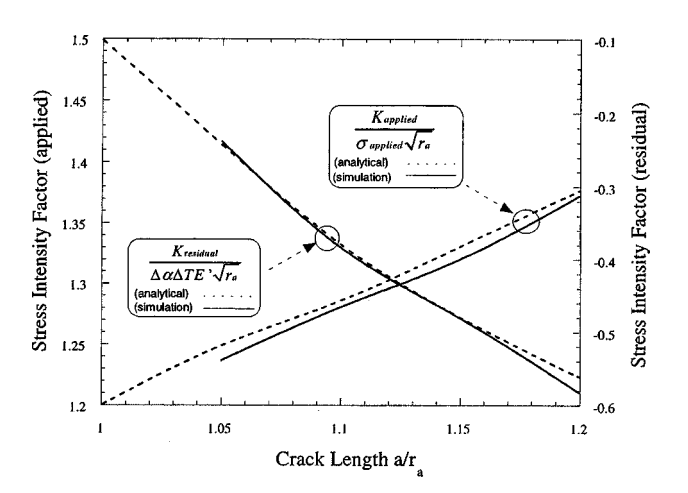


Fig. 7 Comparison of calculated and theoretical stress intensity factors. Thickness of compressive layer is one tenth the diameter of the tensile zone. Diameter of tensile zone is  $2r_a = 450 \ \mu m$ .

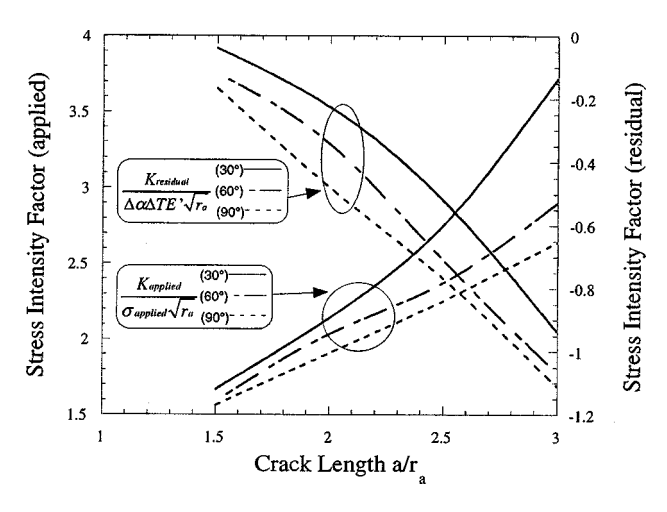


Fig. 8 Comparison of calculated and theoretical stress intensity factors. Tensile and compressive layers have equal thicknesses. Thickness of tensile layer is  $2r_a$ = 200  $\mu$ m.

Figure 8 shows the calculated stress intensity factors for the thickness ratio of  $t/2r_a = 1$ . Again, the results are shown separately for  $K_{\rm applied}$  due to the externally applied load, and  $K_{\rm residual}$  due to the material mismatch. The results are shown for three values of angle  $\theta$ , 30 deg, 60 deg, and 90 deg. As expected, and suggested by Eq. (9), the stress intensity factor decreases as the angle  $\theta$  increases.

Figure 9 shows the calculated stress intensity factors for the thickness ratio of  $t/2r_a = 1/10$ , also for the same three values of angle  $\theta$ , 30 deg, 60 deg, and 90 deg.

Now that the stress intensity factors have been calculated, the next step in our analysis is the determination of threshold strength, which we take up in the following section.

#### 4 Discussion of Threshold Strength

As discussed in Sec. 2.1, the stress intensity factor generally decreases as the crack extends into the compressive layers. Thus, the maximum stress needed to drive the crack through the compressive layers occurs when the crack is at the interface between the compressive and tensile zones, that is, when  $a = r_a + t = r_b$ . In the context of the superposition concept introduced in Sec. 2.1, we can set  $K = K_{\text{applied}} + K_{\text{residual}} = K_c$ ; hence,  $K_{\text{applied}} = K_c - K_{\text{residual}}$ ,

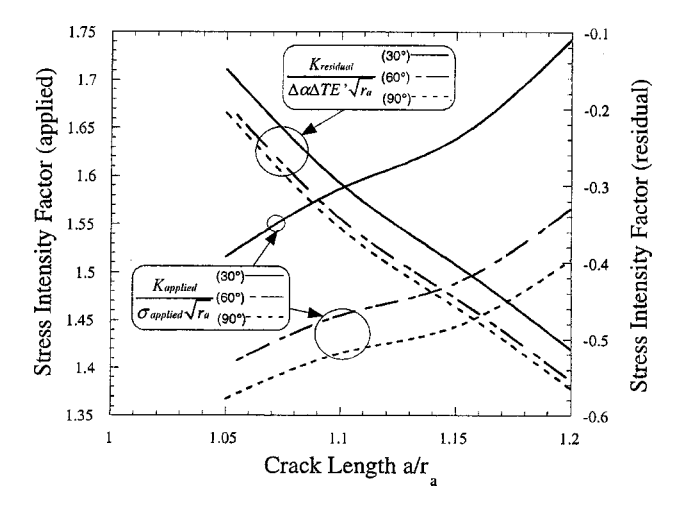


Fig. 9 Comparison of calculated and theoretical stress intensity factors. Thickness of compressive layer is one tenth the diameter of the tensile zone. Diameter of tensile layer is  $2r_a = 450 \ \mu m$ .

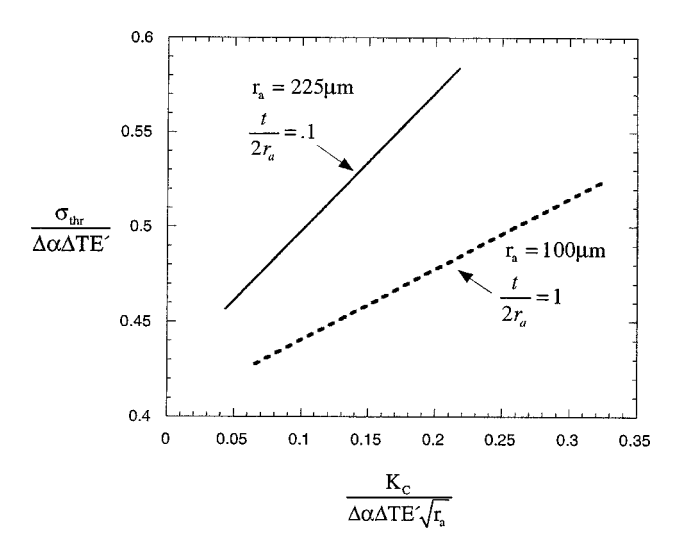


Fig. 10 Threshold strength versus fracture toughness for a full-penny shaped crack

and then solve for the applied stress  $\sigma_a$ , which appears as a linear prefactor in  $K_{\rm applied}$ . Thus, the largest stress needed to extend the crack through the compressive zone is given in a normalized form as:

$$\frac{\sigma_{thr}}{\Delta \alpha \Delta TE'} = \frac{\frac{K_c}{\Delta \alpha \Delta TE' \sqrt{r_a}} - \frac{K_{\text{residual}}(r_b)}{\Delta \alpha \Delta TE' \sqrt{r_a}}}{\frac{K_{\text{applied}}(r_b)}{\sigma_{\text{applied}}\sqrt{r_a}}}.$$
 (11)

If the initial crack size in the tensile layer is less than  $r_a$  and the stress needed to extend it is less than  $\sigma_{thr}$ , the crack will be arrested by the compressive layer. However, if the crack is very small and extends at a stress greater than  $\sigma_{thr}$ , it will extend through the compressive layer and lead to catastrophic failure without being arrested. Thus, Eq. (11) is rigorously thought of as a threshold stress. If the applied stress is less than  $\sigma_{thr}$ , the body should not fail when tensile stress is applied along the fibers. As previously noted, this enables load-bearing components to be designed with the foreknowledge that failure is unlikely to occur below that stress.

As expected, Eq. (11) shows that the threshold strength increases with the fracture toughness of the compressive layers,  $K_c$ . The normalized threshold strengths are plotted in Figs. 10 and 11, against the normalized fracture toughness  $K_c$  of the compressive layer. Values of  $K_c$  are chosen between 1 and 5 MPa $\sqrt{m}$ , a range which is typical of ceramic materials. Values of other material parameters are taken as  $E = 300 \,\text{GPa}$ ,  $\nu = 0.3$ ,  $\Delta \alpha = 2.795$  $\times 10^{-6} \,\mathrm{C}^{-1}$  and  $\Delta T = -1200 \,^{\circ}\mathrm{C}$ , for purposes of setting the ranges of these plot axes. Taking  $K_c = 3 \text{ MPa} \sqrt{\text{m}}$  and  $t/2r_a$ = 1/10, typical of the cylindrical structure by Snyder [10], the threshold strength we arrive at is ~800 MPa. This modestly exceeds what has been observed in that system, but other effects, such as edge cracking and crack branching into other propagation planes (as well as the fact that modulus mismatch is not accounted for here) are being considered as mechanisms that are coming into play in the experimental system.

In addition to the effect of intrinsic fracture toughness, the finite element results reveal the effect of mismatch strain  $\Delta T \Delta \alpha$ , albeit in an indirect way due to the normalization we have chosen to use in Figs. 10 and 11. Inspection of Eq. (11), coupled with the fundamental result that we expect  $K_{\rm residual}$  to vary linearly with  $\Delta T \Delta \alpha$  (and that the  $K_{\rm residual}$  in the numerator of the equation is actually expected to be negative), yields the intuitive result that  $\sigma_{thr}$  increases with mismatch strain.

Transactions of the ASME

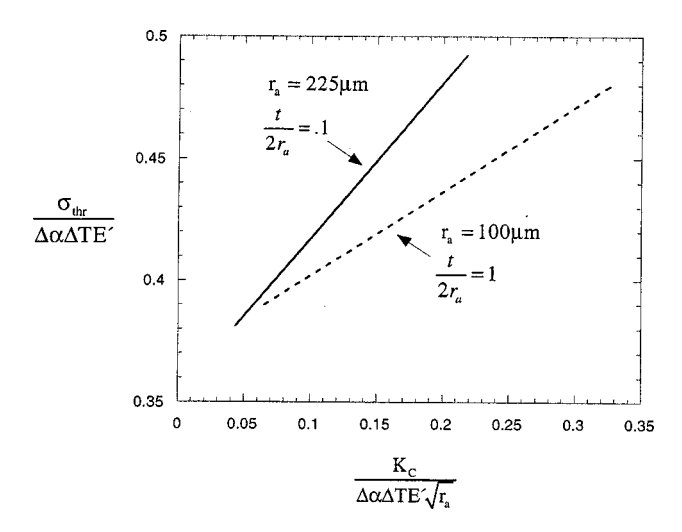


Fig. 11 Threshold strength versus fracture toughness for a half-penny shaped crack. Results are shown for angle  $\theta$ =60°.

The effect of tensile region size  $2r_a$  and compressive layer thickness t, and the ratio  $t/2r_a$ , are even less transparent in the finite element results, simply because we did not perform an extensive parametric study in this space. Nevertheless, useful insight can be gained from the simple analytical model through Eq. (8) which shows that the threshold strength decreases with the thicknesses of the various layers. The ratio  $t/2r_a$  has a modest effect; in addition the absolute size of the tensile zone,  $r_a$ , impacts the threshold stress as well. The latter effect is being exploited by Paranjpye et al. [11] through microelectromechanical systems (MEMS) processing technology to achieve threshold stresses in laminate systems in excess of 1 GPa.

As to be expected, the threshold strength depends on the elastic moduli of the tensile and compressive layers. With everything else held fixed, if the tensile layer were more stiff than the compressive layer, the magnitude of the residual stress rises and hence the threshold strength increases as is apparent from Eq. (7). While we have not performed a systematic study of cases where the compressive layer elastic properties differ from those in the tensile zones, the good agreement that has been observed in this study between the FEM results and the analytic results provide the necessary confidence necessary to build elastic mismatch into future implementations of this FEM model. In addition, more sophisticated procedures, such as considering a periodic structure based on a hexagonal compressive layer configuration (depicted in Fig. 1), and using the J-integral to calculate stress intensity factors, should be explored.

#### 5 Summary

The finite element method was used to predict threshold strengths in a model system consisting of a cylindrical jacket under residual compression, surrounded by regions of tensile material, subject to tensile loading aligned with the cylindrical major axis. The model system has relevance to ceramic composites that have been fabricated by consolidating fibers of one phase in another at high temperature, followed by cooling, resulting in residual compression in the phase surrounding the original fibers. The architecture offers superior mechanical response, in that cracks which originate in the cylindrical zones may be arrested by the surrounding compressive layers, resulting in a truncation of the strength distribution with respect to flaw size and an associated design threshold strength. A simple fracture mechanics model, valid for similar elastic properties is presented, and the finite element results are in good agreement with that analysis. Moreover, the finite element model is extended to the case of a half-penny crack emanating from a traction-free surface. As expected from prior experience with laminate systems, the threshold strength is shown to depend on the mismatch strain (through the thermal expansion coefficient mismatch and temperature change), the intrinsic toughness of the constituent materials, and the thickness ratio. The results are in modest agreement with experimental results.

#### Acknowledgments

The authors would like to thank Fred Lange, Mark Snyder, and Geoff Fair for illuminating discussions.

#### Appendix A

In this Appendix, we overview the derivation of the background stress field that drives crack propagation in the cylindrical, axisymmetric problem discussed in this paper. Consider the geometry depicted in Fig. 2, albeit without a crack. The elastic moduli are taken as identical in all three layers. The coefficient of thermal expansion in the interior layer (of thickness t) is taken as  $\alpha_b$ , and that in the remaining layers is taken as  $\alpha_a$ . The stress equilibrium equations, written in cylindrical coordinates and assuming no body forces, reduce to

$$\frac{\partial \sigma_{rr}}{\partial r} + \frac{1}{r} (\sigma_{rr} - \sigma_{\theta\theta}) = 0$$

$$\frac{\partial \sigma_{zz}}{\partial z} = 0.$$
(A1)

Moreover, compatibility requirements dictate that

$$\frac{\partial}{\partial r}(r\varepsilon_{\theta\theta}) = \varepsilon_{rr}. \tag{A2}$$

Equation (A2) follows from the fact that displacements in the  $\theta$  direction vanish, and the displacement component in the r direction may only depend on r. In addition, we insist that  $\varepsilon_{zz}$  remain constant throughout the structure. Hooke's Law is written as

$$\varepsilon_{rr} = \frac{1}{E} \left[ \sigma_{rr} - \nu (\sigma_{\theta\theta} + \sigma_{zz}) \right] + \alpha_i \Delta T$$

$$\varepsilon_{\theta\theta} = \frac{1}{E} \left[ \sigma_{\theta\theta} - \nu (\sigma_{rr} + \sigma_{zz}) \right] + \alpha_i \Delta T, \tag{A3}$$

$$\varepsilon_{zz} = \frac{1}{E} \left[ \sigma_{zz} - \nu (\sigma_{\theta\theta} + \sigma_{rr}) \right] + \alpha_i \Delta T$$

with the subscript on  $\alpha$  taken to coincide with the appropriate phase. The symmetry of the deformation dictates that all shear quantities vanish.

Inserting  $\varepsilon_{rr}$  and  $\varepsilon_{\theta\theta}$  from Eq. (A3) into Eq. (A2), and eliminating  $\sigma_{\theta\theta}$  via Eq. (A1), yields a linear ordinary differential equation for  $\sigma_{rr}$  that leads to a general solution of the form

$$\sigma_{rr} = C_1 + C_2/r^2; \quad \sigma_{\theta\theta} = C_1 - C_2/r^2,$$
 (A4)

where the constants  $C_1$  and  $C_2$  must be determined separately for each phase, resulting in six (6) unknowns. We note that Eq. (A4) is constant with a piecewise constant solution for  $\sigma_{zz}$ , consistent with the second part of Eq. (A1). Additional boundary conditions are imposed in order to determine the constants: (1) the stress components must remain finite as  $r{\to}0$ ; hence,  $C_2$  vanishes for the inner phase; (2) the outer surface of the structure is free of traction; hence,  $\sigma_{rr}$  is taken as zero at  $r{=}r_c$ ; (3) continuity of  $\varepsilon_{\theta\theta}$  is enforced at both  $r{=}r_a$  and  $r{=}r_b$ ; and (4) continuity of  $\sigma_{rr}$  is enforced at both  $r{=}r_a$  and  $r{=}r_b$ .

There remains a seventh unknown, the constant value of  $\varepsilon_{zz}$ , which is found through a macroscopic force balance. That is, St. Venant's principle is exploited to write

$$\pi r_a^2 \sigma_{zz} (0 \le r < r_a) + \pi (r_b^2 - r_a^2) \sigma_{zz} (r_a \le r < r_b)$$

$$+ \pi (r_c^2 - r_b^2) \sigma_{zz} (r_b \le r \le r_c) = 0.$$
(A5)

With the unknowns in hand, the third of Eq. (A3) may be used to write the longitudinal stress in each phase:

$$\sigma_{zz} = \begin{cases} \frac{E\Delta T(\alpha_b - \alpha_a)(r_b^2 - r_a^2)}{(1 - \nu)r_c^2} & \text{for } 0 \leq r < r_a \\ \frac{E\Delta T(\alpha_b - \alpha_a)(r_b^2 - r_a^2 - r_c^2)}{(1 - \nu)r_c^2} & \text{for } r_a \leq r < r_b. \\ \frac{E\Delta T(\alpha_b - \alpha_a)(r_b^2 - r_a^2)}{(1 - \nu)r_c^2} & \text{for } r_b \leq r \leq r_c \end{cases}$$
(A6)

The solution maps to Eqs. (5) and (6) by substituting  $\Delta \alpha = \alpha_b - \alpha_a$ ,  $r_b = r_a + t$ , and noting that  $\sigma_c = -\sigma_{zz}$  for the sandwiched (compressive) layer.

#### Appendix B

When calculating the threshold strength, it is usually assumed that Eq. (4) decreases continuously throughout the regime  $r_a < a < r_b$ . Taking the first derivative of K(a) and insisting that it must remain negative yields the following restriction:

$$\frac{(\sigma_a + \sigma_t)a\sqrt{a^2 - r_a^2}}{(\sigma_c + \sigma_t)(a^2 + r_a^2)} < 1.$$
 (B1)

We note that the left-hand side of Eq. (B1) increases monotonically in a, so the first location for which the derivative ceases to be negative, at some prescribed level of  $\sigma_a$ , would occur at

 $a = r_a + t$  (i.e., the farthest extent within the compressive zone). Solving Eq. (B1) as an identity gives the critical value:

$$\sigma_{\rm crit} = \frac{(\sigma_c + \sigma_t)(2r_a^2 + 2r_at + t^2)}{(r_a + t)\sqrt{t^2 + 2r_at}} - \sigma_t. \tag{B2}$$

Thus, the stress intensity factor undergoes a minimum within the compressive zone for  $\sigma_a > \sigma_{\rm crit}$ , and Eq. (7) becomes invalid for the threshold strength. By equating Eq. (B2) with Eq. (7), a restriction on material parameters that guarantees stable crack growth across the entire compressive zone can be obtained. Mc-Meeking and Hbaieb [5] have derived similar results for the case of a two-dimensional laminar composite.

#### References

- [1] Green, D. J., 1998, Introduction to Mechanical Properties of Ceramics, Cambridge University Press, Cambridge, UK.
- [2] Lange, F. F., 1989, "Powder Processing Science and Technology for Increased Reliability," J. Am. Ceram. Soc., **72**, pp. 3–15.
- [3] Rao, M. P., Sanchez-Herencia, A. J., Beltz, G. E., McMeeking, R. M., and Lange, F. F., 1999, "Laminar Ceramics That Exhibit a Threshold Strength," Science, 286, pp. 102–105.
- [4] Hbaieb, K., and McMeeking, R. M., 2002, "Threshold Strength Predictions for Laminar Ceramics With Cracks That Grow Straight," Mech. Mater., 34, pp. 755–772.
- [5] McMeeking, R. M., and Hbaieb, K., 1999, "Optimal Threshold Strength of Laminar Ceramics," Z. Metallkd., 90, pp. 1031–1036.
- [6] Lange, F. F., Snyder, M., and Fair, G. (unpublished).
- [7] Tada, H., 1985, The stress analysis of cracks handbook, Paris Productions Inc., St. Louis, MO.
- [8] Raju, I. S., and Newman, J. C., 1979, "Stress-Intensity Factors for a Wide Range of Semi-Elliptical Surface Cracks in Finite-Thickness Plates," Eng. Fract. Mech., 11, pp. 817–829.
- [9] ANSYS, V.5.7, ANSYS Inc., Canonsburg, PA.
- [10] Snyder, M. (private communication).
- [11] Paranjpye, A., MacDonald, N. C., and Beltz, G. E., "Modeling and Simulation in Materials Science and Engineering," in press.